CORE
Metadata, citation and similar papers at core.ac.uk
Provided by DSpace@MIT

Elimination of LWD (Logging While Drilling) Tool Modes using the Seismoelectric Data

Xin Zhan, Zhenya Zhu, Shihong Chi, Rama Rao, Daniel R. Burns and M. Nafi Toksöz
Earth Resources Laboratory
Dept. of Earth, Atmospheric and Planetary Sciences
Massachusetts Institute of Technology
Cambridge, MA , 02139

Abstract

Borehole acoustic logging-while-drilling (LWD) for formation evaluation has become an indispensable part of hydrocarbon reservoir assessment (Tang et al., 2002; Cittá et al., 2004; Esmersoy et al., 2005). However, the detection of acoustic formation arrivals[1] over tool mode contamination has been a challenging problem in acoustic LWD technology. This is because the tool mode contamination in LWD is more severe than in wireline tools in most geological environments (Tang et al., 2002; Huang, 2003).

In this paper we propose a new method for separating tool waves from formation acoustic waves in acoustic LWD. This method is to measure the seismoelectric[2] signal excited by the LWD acoustic waves.

The acoustic waves propagating along the borehole or in the formation can induce electric fields. The generated electric field is localized around the wave pulses and carried along the borehole at the formation acoustic wave velocity. The LWD tool waves which propagate along the rigid tool rim can not excite any electric signal. This is due to the effectively grounding of the drill string during the LWD process makes it impossible to accumulate any excess charge at the conductive tool – borehole fluid interface. Therefore, there should be no contribution by the tool modes to the recorded seismoelectric signals.

In this study, we designed the laboratory experiments to collect simulated LWD monopole and dipole acoustic and seismoelectric signals in a borehole in sandstone. By analyzing the acoustic and electric signals, we can observe the difference between them, which are the mainly tool modes and noise.

---

[1] In this paper, acoustic LWD measurement or signal is composed of formation acoustic waves (modes or arrivals) which are the waves propagating along the formation and tool waves (modes) which are waves propagating along the tool.

[2] Seismoelectric signal refers to the electric field induced by seismic (acoustic) waves.

Then we calculate the similarity of the two signals to pick out the common components of the acoustic and seismoelectric signals, which are the pure formation modes. Using the seismoelectric signals as reference, we could filter out the tool modes. The method works well.

To theoretically understand the seismoelectric conversion in the LWD geometry, we also calculate the synthetic waveforms for the multipole LWD seismoelectric signals based on Pride's theory (Pride, 1994). The synthetic waveforms for the electric field induced by the LWD-acoustic-wave along the borehole wall demonstrate the absence of the tool mode, which is consistent with the conclusions we get in the experimental study.

1. Introduction

1.1 Electrokinetic phenomena

When a fluid electrolyte comes into contact with a neutral solid surface, anions from the electrolyte are chemically absorbed to the wall leaving behind a net excess of cations distributed near the wall. The region is known as the electric double layer (Pride and Morgan, 1991). The first layer of cations is bound to the anion / solid surface. Beyond this first layer of bound cations, there is a diffuse distribution of mobile cations whose position is determined by a balance between electrostatic attraction to the absorbed layer and diffusion toward the neutral electrolyte. The separation between the mobile and immobile charge is called the shear plane. The zeta potential, ζ, is the electric potential at the shear plane, and the electric potential in neutral electrolyte (no excess charge) is defined to be zero (Pride and Morgan, 1991; Bockris and Reddy, 2000). It is normally assumed that the diffuse distribution of mobile charge alone gives rise to the electrokinetic phenomenon and the absorbed layer does not contribute to the electrokinetic phenomenon.

When acoustic waves propagate through a fluid-saturated porous medium, a relative fluid-solid motion is generated (the motion of pore fluid with respect to the solid matrix). This pore fluid relative motion in rocks will induce a streaming electric field due to the electrical charges concentrated in the electric double layer (EDL) (Pride and Morgan, 1991; Mikhailov, 1998). This electric field is a localized one induced by the pressure front of the propagating acoustic wave and posses the same appearant velocity as the acoustic wave (Zhu and Toksöz, 1998).

Conversely, when an electric field induces relative motion of the free charges in the pore fluid against the solid matrix, the interaction between the pore fluid and the solid matrix generates an acoustic wave. This process is the electroseismic conversion (Thompson and Gist, 1993; Pride and Haartsen, 1996). The electroseismic waves have been observed in laboratory experiments (Zhu et al., 1999) as well.

1.2 Acoustic logging-while-drilling (LWD)

Acoustic logging-while-drilling (LWD) technology was developed in the 1990's to meet the

demand for real-time acoustic logging measurements for the purpose of providing seismic tie or / and acoustic porosity and pore pressure determination (Aron et al., 1994; Minear el al., 1995; Market et al., 2002; Tang et al., 2002; Cittá et al., 2004). The LWD apparatus, with sources and receivers located close to the borehole wall and the drill collar taking up a large portion of the borehole, have some significant effects on borehole acoustic modes.

The actual LWD measurement is complicated by several factors. One major effect is the impact of tool waves. The tool waves are strong in amplitude and always exist in the multipole LWD measurements. These and others noise sources contaminate the true formation acoustic waveforms, causing difficulty in the recognition of formation arrivals. The various vibrations of the drill string in its axial, radial, lateral, and azimuthal directions, together with the impact of the drill string on the borehole wall and the impact of the drill bit on the formation, generate strong drilling noise. Field measurements (Joyce et al., 2001) have shown that the frequency range of this noise influences the frequency range of the measurement of shear wave velocities in slow formations. It is the difficulty in characterizing and removing the source of the noise that has motivated the research in this paper.

2. LWD acoustic and seismoelectric measurements in scaled laboratory experiment

In LWD multipole acoustic logging, both the source and the receiver transducers are tightly mounted on the drill collar. This attachment results in the receivers recording a tool mode propagating along the drill collar. The tool mode can interfere with the acoustic fields propagating along the formation. To simulate the LWD measurement, we built a scaled multipole acoustic tool composed of three parts: the source, receiver, and a connector (Zhu et al., 2004). Working in the ultrasonic frequencies the tool is put into a scaled borehole to measure the monopole and dipole acoustic waves. For the seismoelectric measurements, we only need to change the receiver section from the acoustic transducer array to the electrode array with the same spacing and located at exactly the same location. Thus, we could measure the LWD acoustic and electric signal generated from the same acoustic source approximately along the same path.

2.1 Experimental borehole model

The experiment borehole we use is a homogenous, isotropic block – sandstone. The P- and S-velocities are all higher than the borehole fluid velocity. The sandstone block has a length of 30cm, a width of 29cm, and a height of 23cm. The diameter of the borehole is 1.7cm. For the scaled LWD tool, we use the equivalent composite tool velocity to indicate the steel tool has holes in it to embed acoustic transducers and electrodes. The tool ID is 0.004m, tool OD is 0.01m and borehole radius is 0.017m. All the velocities are shown in Table 1. Schematics of the borehole model are shown in Figure 1.

	P-velocity	S-velocity	Density	Outer Radius
Inner Fluid	1500 m/s	-------	1000 kg/m^3	0.002 m
Tool (Composite)	5800 m/s	3100 m/s	7700 kg/m^3	0.005 m
Outer Fluid	1500 m/s	-------	1000 kg/m^3	0.0085 m
Formation	4660 m/s	2640 m/s	2100 kg/m^3	∞

Table 1. LWD laboratory borehole model parameters.

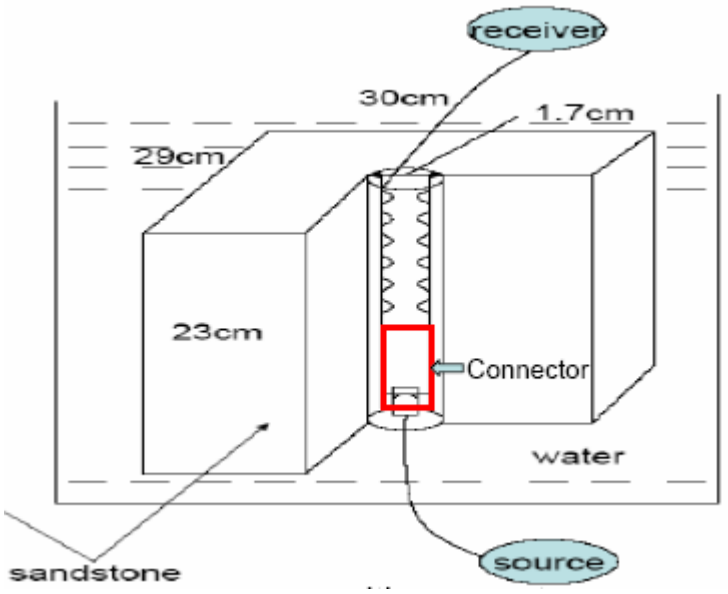

Figure 1. Schematics of the borehole model in the laboratory measurement.

2.2 Structure of the scaled multipole tool in the LWD acoustic measurements

Our laboratory LWD tool includes three sections: the source, the receivers, and the connector. Both the source and receiver acoustic transducers are made of PZT crystal disks of 0.635cm in diameter and 0.37cm in thickness. The dimension of the tool is shown in Figure 2.

The source is made of four separate crystal disks shown in the B-B profile of Figure 2. The arrows on the disks indicate their piezoelectric polarization. Each disk has two electrodes attached to it; the eight electrodes are connected to a switch. Using the switch to change the electric polarization applied on each crystal disk, we can achieve a working combination to simulate a monopole or dipole source. The receiver section is composed of six pairs of crystal disks at six different locations. The polarizations of each disk pair are shown in the A-A profile of Figure 2.The connector section is made of a steel pipe threaded at each end. The source and receiver sections are tightly connected by this steel pipe to simulate the drill-string connection in LWD.

By changing the electric polarization of the source PZT disks and by combining the signals received by the receiver pairs, we are able to simulate a working system of acoustic logging sources. When the piezoelectric polarization of the source transducer is consistent with the positive pulse of the source signal, the phase of the acoustic wave is also positive. The polarization of the received acoustic field is the same as the piezoelectric polarization of the

receiver transducer. The working combinations of monopole and dipole systems are shown in Figure 3.

During measurements, we used a switch to change the working mode from monopole to dipole. This allows us to conduct the multipole logging without changing or moving the tool position. Therefore, the experiment results can be compared under the identical conditions.

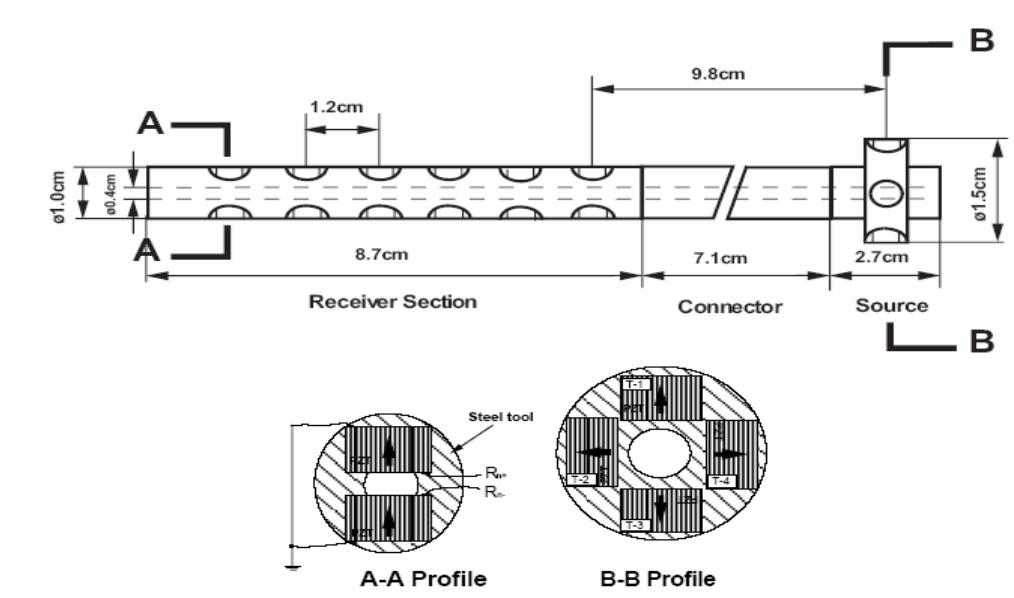

Figure 2. Schematic diagram of the scaled lab multipole tool in LWD acoustic measurement. The arrows indicate the polarization of the PZT disks (Zhu et al., 2004).

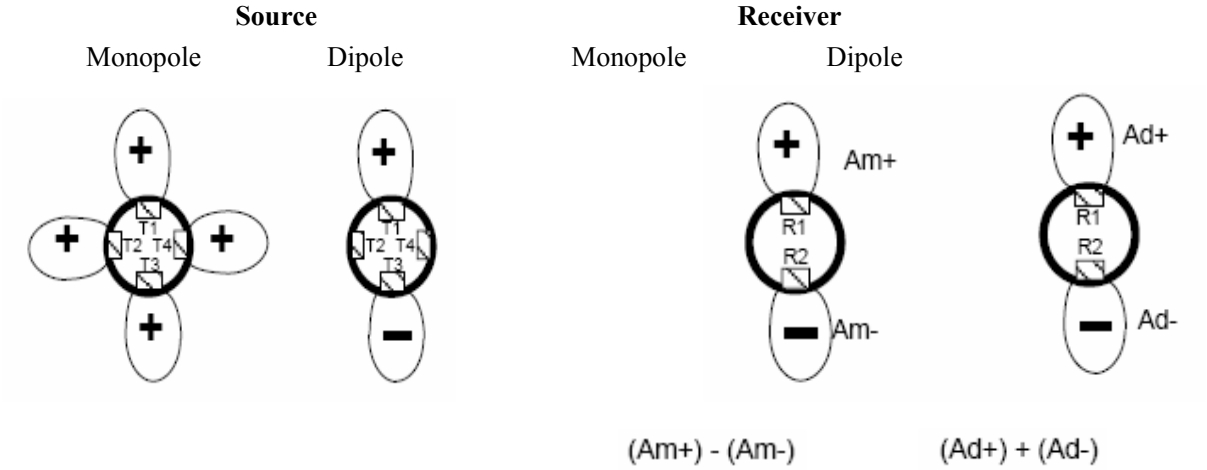

Figure 3. Schematic diagram of the working modes of the multipole logging tool. The "+" and "-" indicate the polarization of the electric signals in the source and the polarization of the PZT crystals in the receiver (Zhu et al., 2004).

2.3 Structure of the scaled multipole tool in the LWD seismoelectric measurements

To measure the seismoelectric signal, we need to change the receiver section from acoustic transducers to electrodes. The electrodes used for this experiment are point electrodes of 1.0mm in diameter. Thus, each electrode on the electrode array can only detect the electric

field around it.

The multipole tool used to measure seismoelectric signals is also composed of three parts: source, receiver and connector. The source section and the connector are exactly the same in structure and size as in the acoustic case. The only change is the replacement of the array of the six pairs of transducers by an array of six pairs of electrodes spaced at the same interval. The holes in which the electrodes are imbedded are filled with sand and glued by epoxy. The surface is covered with conducting glue and connected to the steel tool. The acoustic transducer is embedded in the logging tool as shown in Figure 2 to measure the acoustic pressure at the tool rim. The electrodes are protruding from the tool surface (Figure 4) and are close to the borehole wall to measure the potential difference between the localized electric field at the borehole wall and ground (zero potential).

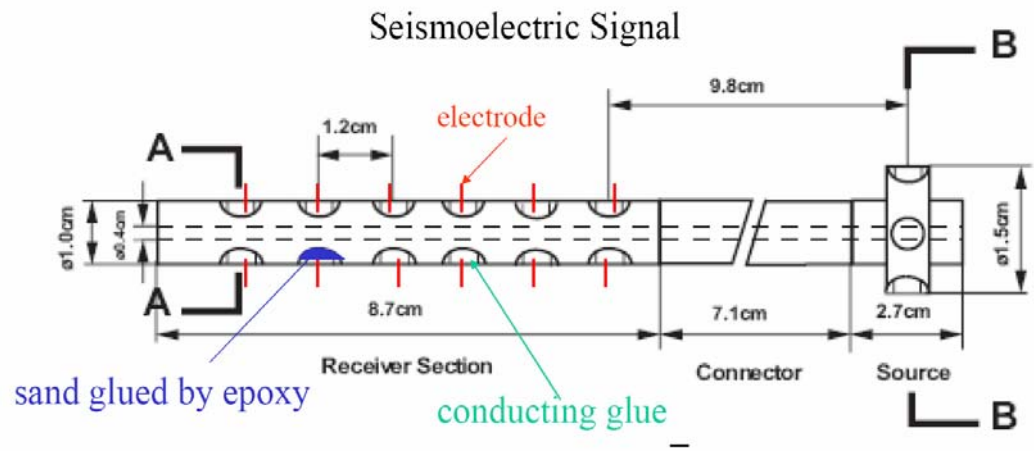

Figure 4. Schematic diagram of the scaled lab multipole tool in LWD seismoelectric measurement.

2.4 Experimental procedure

It is generally accepted that the electric double layer (EDL) is the basis for the electrokinetic conversion (Pride and Morgan, 1991; Loren et al., 1999). For our sandstone borehole model, an EDL is developed at the borehole formation – borehole fluid interface. When the acoustic waves hit the borehole wall, a localized electric field is generated and the electrode detects this electric field. Since the conductivity of the borehole fluid is very low, the recorded voltage between the electrode and ground can represent the electric field generated at the borehole wall. The difference between rock and steel tool is that the latter one is a conductor. By effectively grounding of the drilling collar during the real LWD process, there could be no excess charge accumulation at the steel tool surface. Though the tool waves propagate along the rigid tool surface with a large amplitude, no excess charge can be moved by the tool wave pressure to induce a localized electric field at the tool – borehole fluid interface. Thus, in the seismoelectric signals, what we record are purely the electric fields excited by the formation acoustic waves propagating along the borehole wall and with the velocities of formation acoustic modes.

Before starting an experiment, the sandstone borehole model with a vertically drilled hole is lowered into a water tank. The source and receiver sections are put into the borehole from

two sides with the connector in place. The source side is connected to a high voltage generator and the receiver side to a preamplifier and a filter before being displayed on an oscilloscope. The working system is shown in Figure 5. The High Power Pulse Generator generates a square pulse with a center frequency of 100 kHz. The excitation voltages for the measurements vary between 5 volts and 750 volts. The sampling rate is 500 ns. For each trace we record 512 points. The filter range set from 500 Hz to 300 kHz is broad enough to include all the dominant acoustic and electric modes.

We first measure the monopole and dipole tool modes for calibration of our laboratory tool by firing the tool in the water tank. Then we put the tool in the borehole to record the LWD monopole and dipole acoustic waves. After the measurements for the acoustic signals, the acoustic receiver transducers are replaced by electrodes to make the seismoelectric measurements. We put the grounded tool into the water tank again to test if any seismoelectric signal can be observed. In the end, we focus on the LWD seismoelectric signal measured in the sandstone borehole. The waveforms and analysis results of following measurements will be presented in the following sequence in the next section:

1)acoustic tool waves in the water tank
2) seismoelectric signals with the grounded tool in the water tank
3) LWD acoustic signals in the sandstone borehole
4) LWD seismoelectric signals in the sandstone borehole.

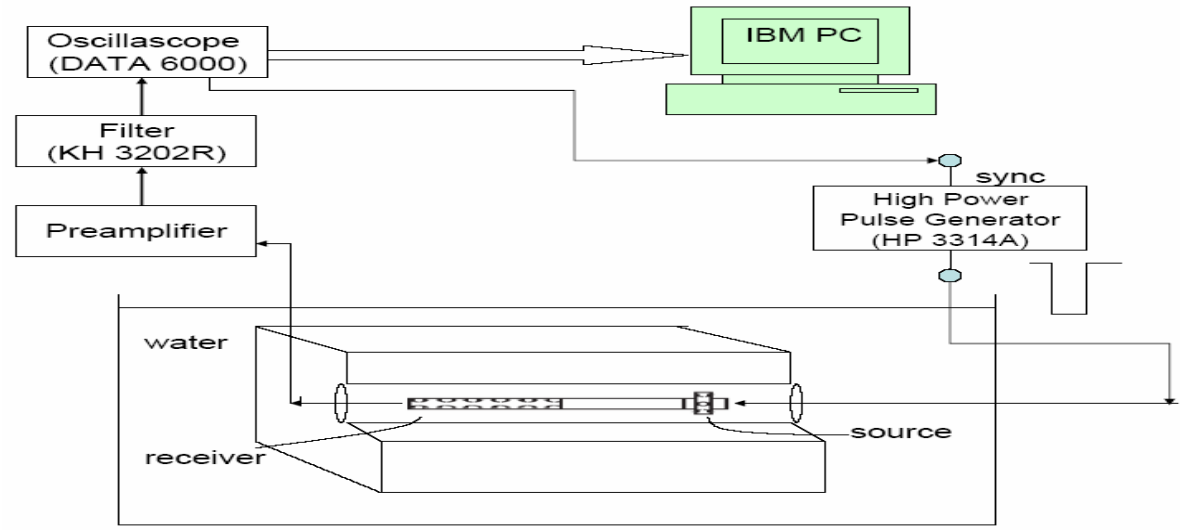

Figure 5. Schematic diagram of the experiment working system (The source wavelet from the High Power Pulse Generator is a square wave).

3. Analysis of laboratory acoustic and seismoelectric signals

In this section, we analyze the acoustic and seismoelectric signals obtained in our laboratory experiments to achieve three objectives: 1) studying of the acoustic LWD signal generated by our scaled lab tool in the lab borehole geometry; 2) understanding the seismoelectric phenomena in the LWD process; 3) investigating the potential application of the LWD

seismoelectric signals. We use an array processing method to analyze the recorded acoustic and seismoelectric signals. We then assess the impact of tool modes on LWD acoustic measurements. Finally, we observe the difference between LWD acoustic and seismoelectric signals and use the seismoelectric signal as a filter to separate out the tool modes from the formation acoustic modes in acoustic LWD signals.

3.1 Array processing methods and noise reduction issues

To analyze the experimental acoustic and seismoelectric signal, we will apply the semblance method which is commonly used in the modern acoustic logging. Time domain semblance algorithm searches for all arrivals received by the array and locates the appropriate wave arrival time and slowness values that maximize the coherent energy in the array waveforms(Kimball and Marzetta, 1984).

The electric data in the experiment is recorded by the point electrodes exposed in water. The signal is rather weak, therefore can be contaminated by the ambient electric fields (Butler and Russell, 1993, 2003; Russell et al., 1997). This ambient noise not only contaminates the electric waveforms but also reduces the ability of the semblance method to recognize the wave modes. In order to reduce noise and enhance the signal to noise ratio (SNR) of the electric signal, steps need to be taken both during the data collection process and during analysis.

To reduce random noise, we sum the repeated measurements. The averaging function of the oscilloscope is used for summing. Each trace in electric array data is the average of 512 sweeps. Good shielding to eliminate the outside noise is also very important for weak signal detection. Some good practices include the following: effectively grounding the computers, oscilloscope, and the shielding line of the point electrode; placing the transducers and electrodes completely in water; shutting down unnecessary electric sources; grounding the water tank, etc.

Besides random noise, we also have a large synchronous signal radiated from the source (high power pulse generator) and a DC component in the electric recordings. This synchronous signal is large in amplitude and appears in front of the wave train so that a lot of useful modes may be buried in the large noise. Fortunately, the source noise does not have a phase move-out over the receiver array, while the seismoelectric signals do. We can subtract the mean value of the six source – receiver offsets traces from each individual trace to eliminate this noise. The DC component can be eliminated with a high-pass filter for each trace seperately.

3.2 Acoustic and seismoelectric signals with tool in the water tank

In order to understand the acoustic properties of monopole and dipole tool modes of our specific scaled multipole tool, we first conduct measurements by putting the tool into the water tank, in the absence of the borehole formation. We make the measurements when the tool is vertically placed in the water tank and grounded to obtain the monopole tool wave (speed at 3400 m/s) and the dipole tool wave (speed about 900 m/s).

Next, we change the receiver section from the acoustic transducer array to the electrode array after we measure the tool wave velocity with the tool in the water tank. Both the acoustic and seismoelectric signals with the tool in the water tank are shown in Figure 6. From the waveform and time domain semblance in Figure 6, we're confident in drawing the conclusion that even though there're strong tool waves propagating along the drilling collar, no electric signal are generated at the tool – fluid interface due to the effective grounding of the steel tool.

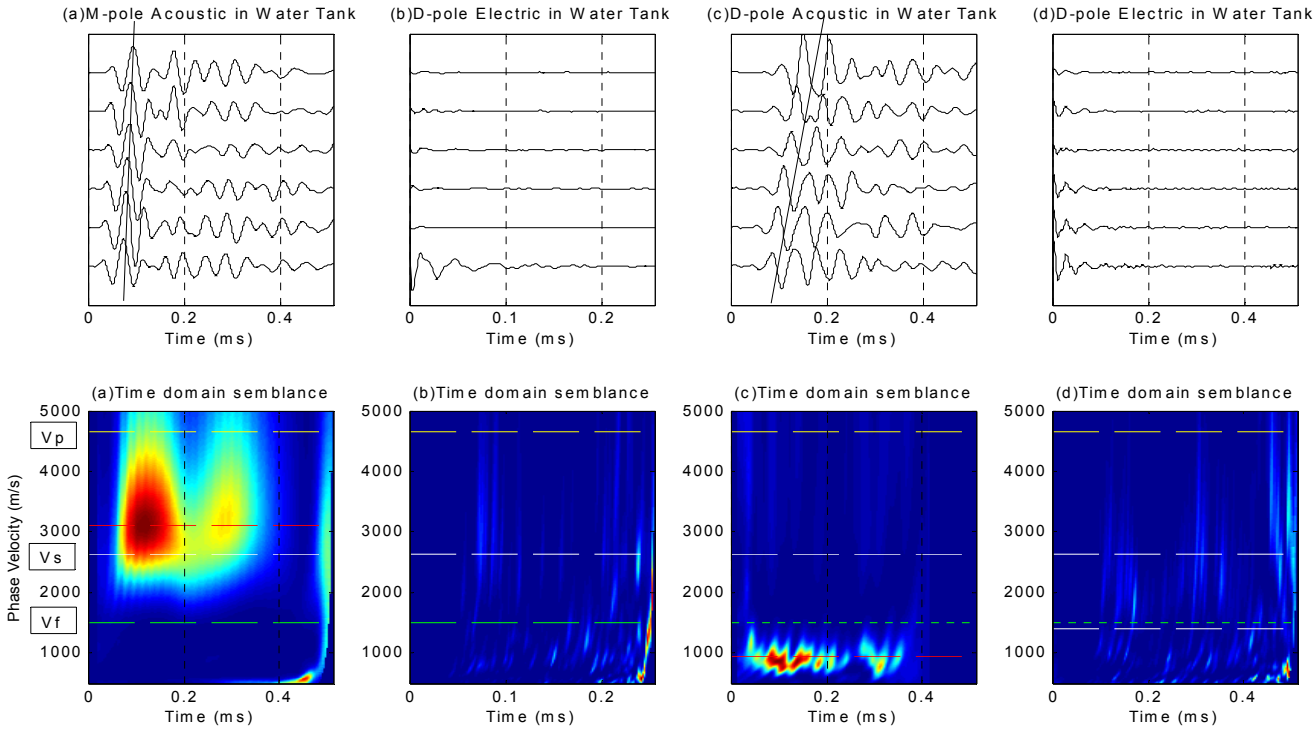

Figure 6. Acoustic and seismoelectric signals with the tool in the water tank. (M-pole stands for monopole, D-pole stands for dipole. The yellow, white, green and red lines indicate the formation P, S and fluid, tool velocities respectively)

3.3 LWD acoustic and seismoelectric signals in the sandstone borehole

Now we will focus on the difference between the LWD acoustic and seismoelectric signals in the sandstone borehole model. As pointed out previously, the seismoelectric signal excited in the acoustic LWD process should contain no signals with the apparent velocity of the tool modes.

We now examine the two kinds of signals for monopole (Figure 7) and dipole (Figure 8) excitations using time domain analysis. From the acoustic waveform we can clearly see a monopole tool wave coming between P and S wave and a low frequency dipole tool wave coming in the late part of the wave train. In the time domain semblance we can observe the peaks at the monopole and dipole tool waves. In the seismoelectric data, tool modes do not exist. Of course, the velocity of the tool modes may slightly change due to the borehole

environment. These results show that by measuring the seismoelectric signal during the logging-while-drilling process, we can potentially eliminate the effect of tool modes.

Based on the laboratory experiments we conclude the following:

LWD acoustic signal = Formation acoustic waves + Tool waves + Noise

LWD SEL signal = Formation acoustic wave induced electric signals + Noise.

In field acoustic LWD operation, the tool modes can have velocities close to the formation velocities for some formations. Therefore, the detection of formation arrivals can be hampered by tool mode contamination. The seismoelectric signal in the LWD process, do not contain tool mode induced electric signals. Given that the LWD acoustic and seismoelectric (SE) signals are different in content, we can use the SE signal to filter the acoustic signal to eliminate the tool modes. The idea can be illustrated in Diagram 1.

We measure the similarity between the acoustic and SE signals using their respective spectra. There are several reasons for this to be done in the frequency domain instead of the time domain. ① In the frequency range where the formation acoustic wave modes exist, the waveforms overlap better. In other frequency ranges where the waveforms differ greatly due to the different modes content, it is difficult to find the correlation between the two signals. ② There are phase difference between the two signals due to the various circuit elements used in laboratory collection of the two signals and the seismoelectric coupling. ③ In the acoustic record, it takes time for the main acoustic energy to propagate from the borehole wall to the receiver transducer at the fluid acoustic velocity. While the propagation time for the electric signal can be ignored due to the high EM wave speed. Thus, it is more difficult to compare the two signals in time domain than in the frequency domain.

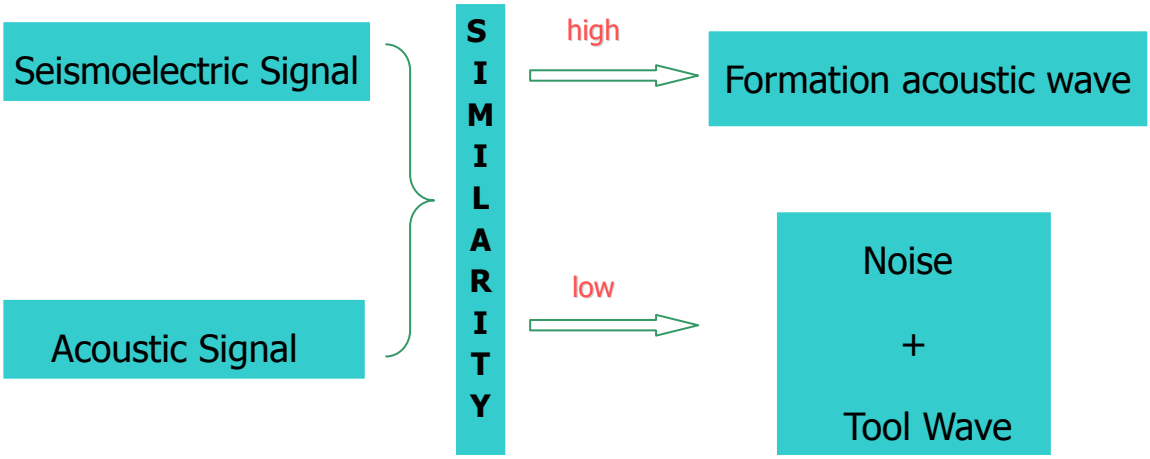

Diagram 1. LWD acoustic and seismoelectric signal coherence

To find the similarity in frequency domain, we first apply the fast fourier transform (FFT) to calculate the amplitude spectra of the two signals, which is the average of the spectra of the six traces in both signals. We then calculate the similarity coefficients of the two frequency curves defined by

$$r = \frac{\sum_m A_m B_m}{\sqrt{\sum_m (A_m)^2 (B_m)^2}} \qquad (3.1)$$

,where A_m and B_m are the acoustic and electric amplitude spectrum, m is the index of the sampling point in frequency domain. A moving window is used to scan the spectra of the two signals simultaneously. The similarity coefficient of that window is set to be the similarity for the center frequency of the window.

The similarity curves and the filtered results are shown in Figure 9 for monopole excitation and Figure 10 for dipole excitation. In Figure 9, ST stands for Stoneley wave, T stands for monopole tool wave. In Figure 10, F stands for dipole flexural wave, T stands for dipole tool wave. The monopole similarity curve is similar to a band stop filter. The dipole coherence curve is similar to a band pass filter.

After obtaining a coherence curve (Figure 9b, Figure 10b), we use it to design a zero-phase filter to be applied to the acoustic signal. A time domain semblance for the filtered data is then computed. We can see clearly that the filtered data contains only formation acoustic modes (Figure 9c, Figure 10c). Other benefits of this filtering method include the reduction of noise in the acoustic signal as well. To further demonstrate these benefits, we detect the peaks in the acoustic and seismoelectric signal spectra and calculate the corresponding wave velocity of those frequency peaks. We find that in the frequency range with low similarity the wave velocities are also different, which means the wave modes are different.

The above analysis illustrates that by correlating the LWD seismoelectric signal with the acoustic signal, we can pick out formation acoustic modes from the LWD acoustic measurement and reduce the noise. This is a very significant result for extracting the formation arrivals from real-time LWD field data that may be contaminated by the complex tool modes and the drilling noise.

Besides the laboratory experiments, we could theoretically understand the seismoelectric conversion in the LWD geometry by developing a Pride-theory-based model for the LWD-acoustic-wave induced electric fields as well. In the theoretical modeling, we could set the vanishing of the electric field at the LWD tool surface to be the boundary condition. This reveals the basic mechanism in the LWD seismoelectric conversion. The synthetic LWD electric waveforms confirm the absence of tool modes, which is consistent with our experimental results. The details of the theoretical model and results are demonstrated in Appendix A.

4. Conclusion

In this paper, we studied the electric fields induced by borehole monopole and dipole LWD acoustic waves both experimentally and theoretically. We developed laboratory experimental set-up and procedures as well as processing methods to enhance the recorded seismoelectric signal. A Pride-theory-based model for the acoustic wave induced electric field in the LWD geometry can also be used to calculate the electric field strength excited by the acoustic pressure. A suite of acoustic and seismoelectric measurements are made to demonstrate and

understand the mechanism of the borehole seismoelectric phenomena, especially under LWD acoustic excitation.

We measured both acoustic and seismoelectric signals under exactly the same settings in our scaled laboratory borehole. The acoustic property of the scaled experimental tool and the formation response were examined first to validate the tool's characteristics. The effects of tool modes on the acoustic LWD signal were illustrated. We analyze the experimental LWD acoustic and seismoelectric signals. The difference between these two signals are the tool modes. We showed that the tool modes can be filtered out by using a filter designed from the similarity curve of the two signals.

Summarizing the whole paper, the following two conclusions can be reached:

1. LWD seismoelectric signals do not contain contributions from tool modes.
2. By correlating the LWD seismoelectric and acoustic signals, we can effectively separate the real acoustic modes from the tool modes and improve the overall signal to noise ratio in acoustic LWD data.

This paper has taken the first step towards understanding borehole LWD seismoelectric phenomena. With future improvements in both theory and instrumentation, seismoelectric LWD could evolve into a robust logging method routinely used in the not-too-distant future.

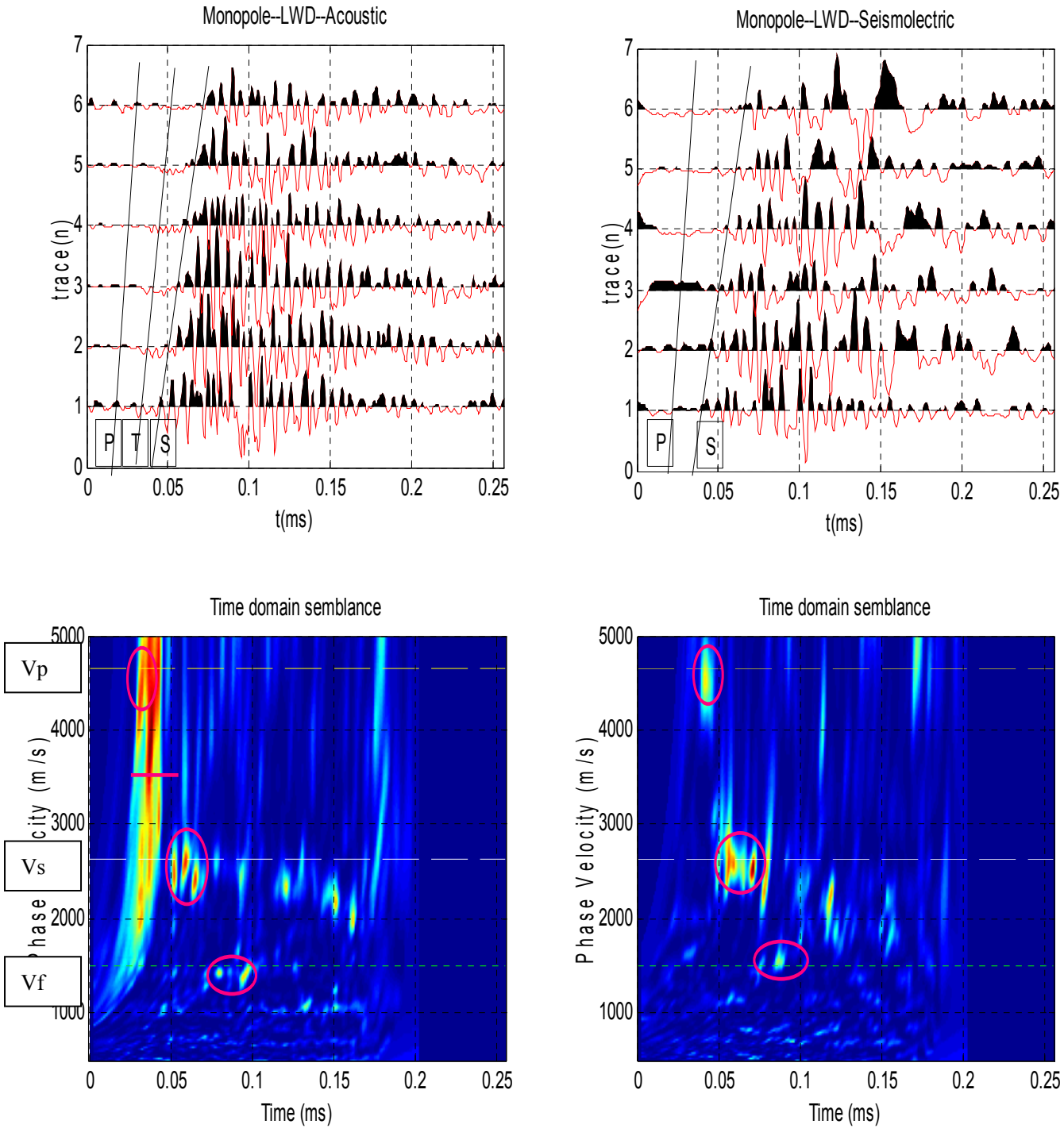

Figure 7 Monopole LWD acoustic (left) and seismoelectric signal (right) comparison. (Vp stands for formation P wave velocity, Vs for formation S wave velocity, and Vf for fluid velocity; P means P wave, S means S wave, T means tool wave.)

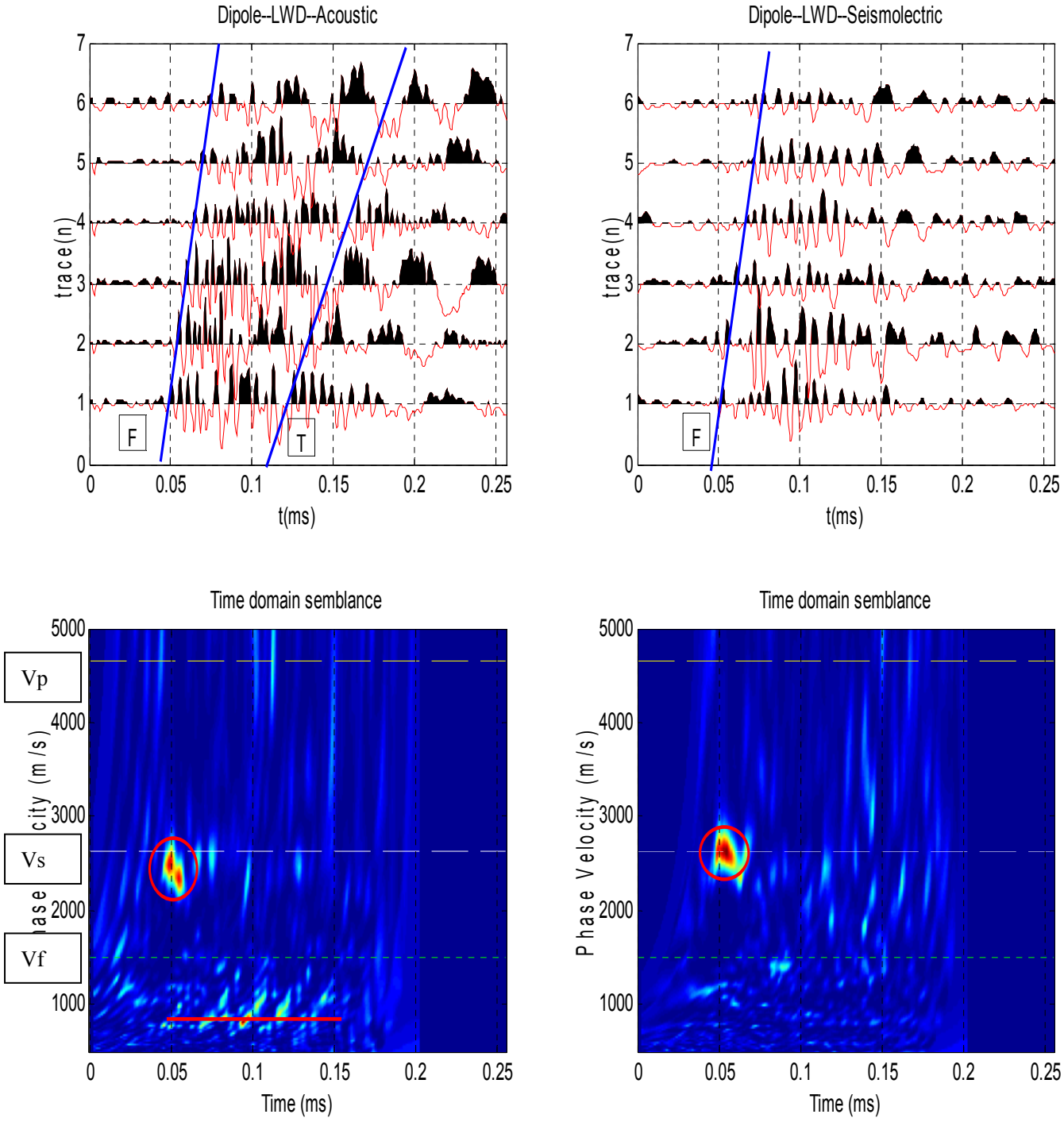

Figure 8 Dipole LWD acoustic (left) and seismoelectric signal (right) comparison. (Vp stands for formation P wave velocity, Vs for formation S wave velocity, and Vf for fluid velocity; F means formation flexure wave, T means tool wave.)

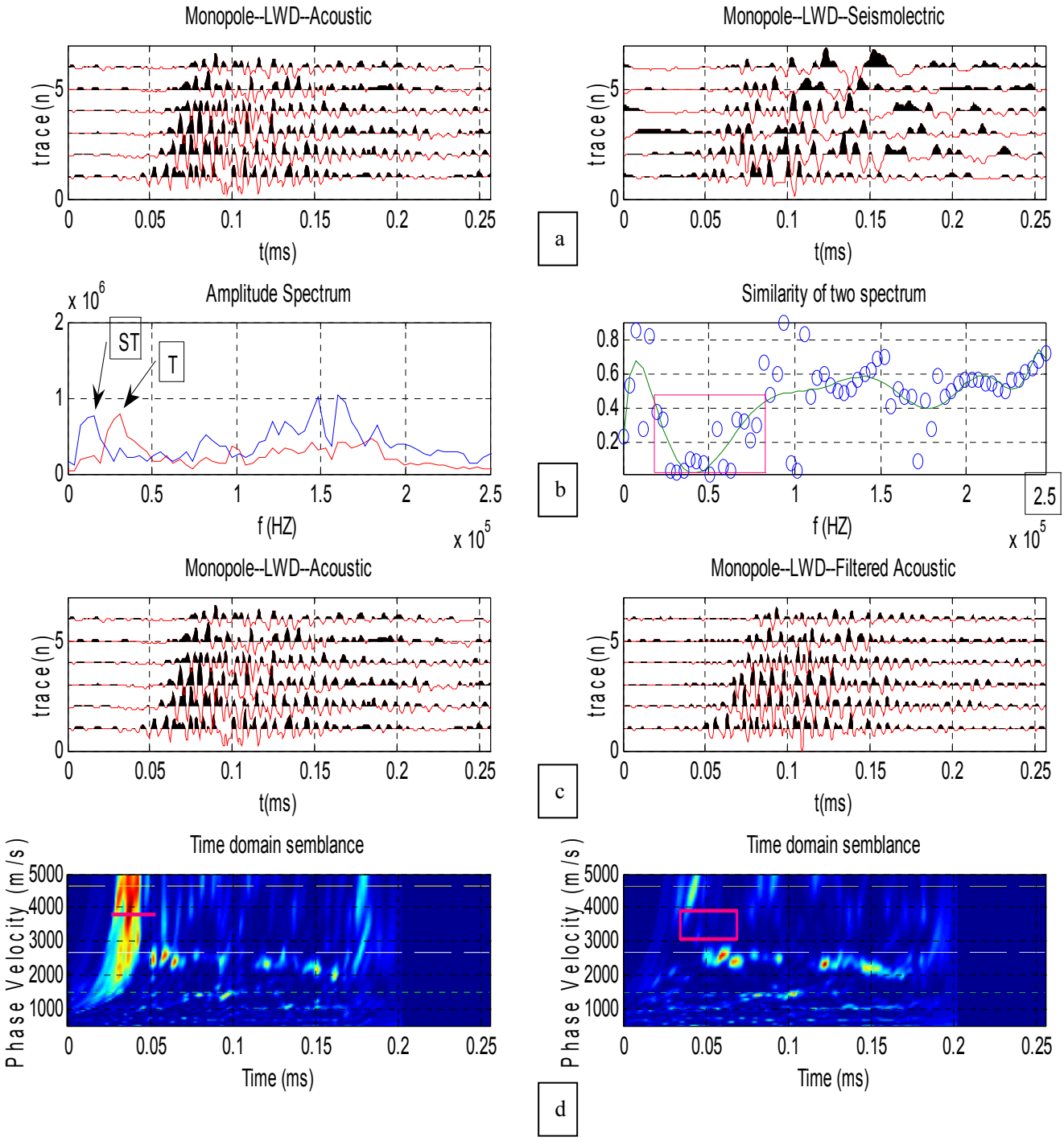

Figure 9 (a) Monopole acoustic (left) and seismoelectric (right) waveforms; (b) monopole acoustic (line with arrow "T") and seismoelectric (line with arrow "ST"). Fourier amplitude spectra (left) and coherence as a function of frequencies (right); (c) monopole unfiltered acoustic (left) and filtered (right) waveforms; and (d) their time domain semblances. (T means frequency peak due to tool wave, ST stands for Stoneley wave).

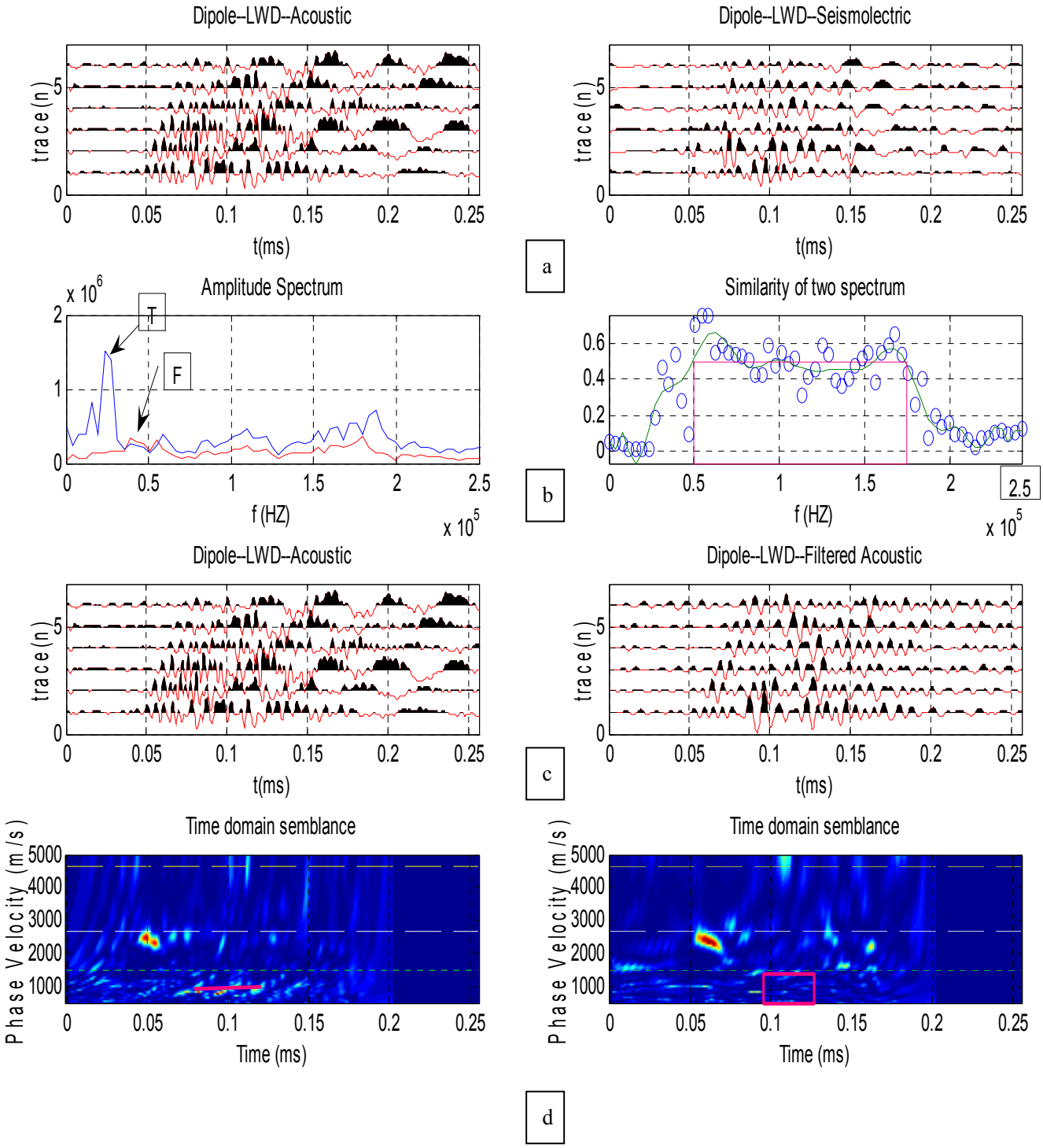

Figure 10 (a) Dipole acoustic (left) and seismoelectric (right) waveforms; (b) dipole acoustic (line with arrow "T") and seismoelectric (line with arrow "F") Fourier amplitude spectra (left) and coherence as a function of frequencies (right); (c) dipole unfiltered acoustic (left) and filtered (right) waveforms; and (d) their time domain semblances. (T means frequency peak due to tool wave, F stands for Flexural wave).

Appendix A

Theoretical modeling of the LWD seismoelectric signal

In this appendix, we apply the Pride's governing equations into the LWD geometry to develop a theoretical model for the LWD-acoustic-wave induced electric field. Both the acoustic pressure and the electric field strength are calculated by matching the acoustic and electric boundary conditions at the three boundaries in our LWD model. The synthetic acoustic and electric waveforms calculated in a slow formation under the dipole excitation clearly demonstrate the absence of the dipole tool modes. It also helps us to understand the relationship between the acoustic pressure and the converted electric field strength as given out in Pride's equations. Finally, we carry out numerical calculations for our laboratory measurements, described in Table 1, in order to compare the experimental and theoretical results. A consistent conclusion, which is the absence of the tool modes in the LWD seismoelectric signals, can be drawn in both experimental and theoretical results.

A.1 Acoustic wave propagation in the logging-while-drilling

Before we couple the electric field into the LWD geometry, we will first give out the expressions for the acoustic field in the formation in LWD environment. In total, four layers construct the LWD model as shown in Figure 10.

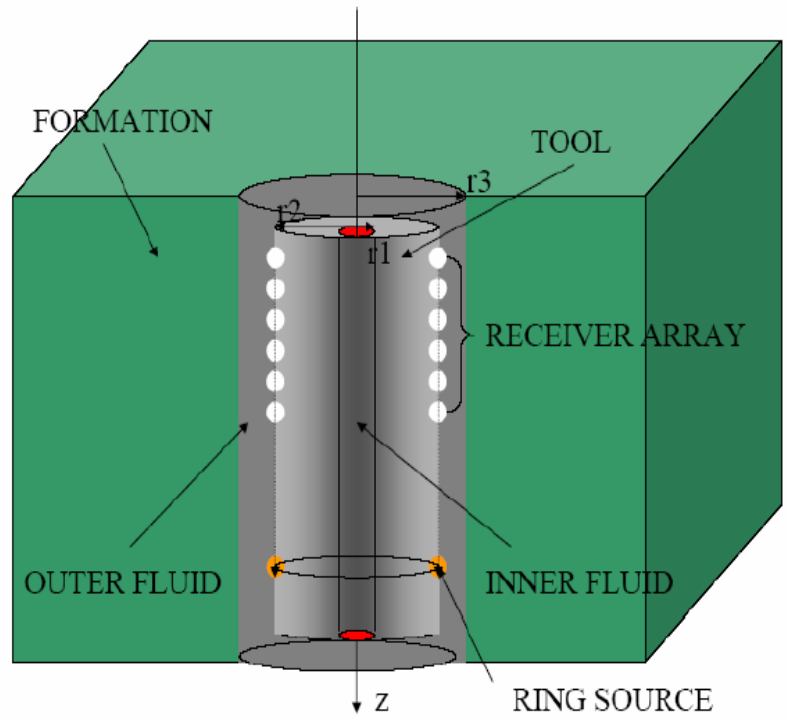

Fig 4.1 Geometry of the borehole and logging tool in the modeling. (r_1, r_2, r_3 indicates the inner fluid , tool outer layer and borehole radius respectively.)

We adopt the cylindrical coordinates (r, θ, z) to express the displacement potentials for

each layer in the LWD geometry in an infinite homogenous elastic formation.

inner fluid layer: $\phi_1 = e^{ikz}\frac{1}{n!}\left(\frac{fr_0}{2}\right)^n A_1 I_n(kp_1 r)\cos(n(\theta-\phi)) \quad (K_n(r\to 0)\to\infty) \qquad (A.1)$

$$\phi 2 = e^{ikz}\frac{1}{n!}\left(\frac{fr_0}{2}\right)^n \left[A_2 I_n(kp_2 r) + B_2 K_n(kp_2 r)\right]\cos(n(\theta-\phi))$$

rigid tool layer: $\chi_2 = e^{ikz}\frac{1}{n!}\left(\frac{fr_0}{2}\right)^n \left[C_2 I_n(ks_2 r) + D_2 K_n(ks_2 r)\right]\sin(n(\theta-\phi)) \qquad (A.2)$

$$\Gamma_2 = e^{ikz}\frac{1}{n!}\left(\frac{fr_0}{2}\right)^n \left[E_2 I_n(ks_2 r) + F_2 K_n(ks_2 r)\right]\cos(n(\theta-\phi))$$

outer fluid layer: $\phi_3 = e^{ikz}\frac{1}{n!}\left(\frac{fr_0}{2}\right)^n \left[A_3 I_n(kp_3 r) + B_3 K_n(kp_3 r)\right]\cos(n(\theta-\phi)) \qquad (A.3)$

$$\phi_4 = e^{ikz}\frac{1}{n!}\left(\frac{fr_0}{2}\right)^n B_4 K_n(kp_4 r)\cos(n(\theta-\phi))$$

formation layer: $\chi_4 = e^{ikz}\frac{1}{n!}\left(\frac{fr_0}{2}\right)^n D_4 K_n(ks_4 r)\sin(n(\theta-\phi)) \quad (I_n(r\to\infty)\to\infty) \qquad (A.4)$

$$\Gamma_4 = e^{ikz}\frac{1}{n!}\left(\frac{fr_0}{2}\right)^n F_4 K_n(ks_4 r)\cos(n(\theta-\phi))$$

where ϕ_j, χ_j and Γ_j are the compressional, vertically polarized shear wave and horizontally polarized shear wave potential of the *jth* layer respectively; n is the azimuthal order number with $n = 0, 1, 2$ corresponding to monopole, dipole and quadrupole source, respectively; I_n and $K_n(n = 0,1,\ldots)$ are the modified Bessel functions of the first and second kind of order n; ω is the angular frequency; $kp_j = \frac{\omega}{\alpha_j}$ and $ks_j = \frac{\omega}{\beta_j}$ are the compressional and shear wavenumber for the *jth* layer; and α_j and β_j are the compressional and shear velocity, respectively. ϕ is a reference angle to which the point source locations are referred to. And $A_1, A_2, B_2, C_2, D_2, E_2, F_2, A_3, B_3, B_4, D_4, F_4$ are the total 12 coefficients to be decided by the acoustic boundary conditions for the 4 layers indicated by the subscripts. Applying the unbounded boundary conditions to the three boundaries in the LWD geometry, we can solve for the 12 unknowns in equations $(A.1)$ to $(A.4)$. The boundary conditions are the continuity of the radial displacement u and stress

element σ_{rr}, and the vanishing of the other two shear stress elements $\sigma_{r\theta}$ and σ_{rz}.

A.2 The converted electric field in the borehole formation

According to Pride's theory (Pride, 1994; Pride and Haartsen, 1996), the elastic field is coupled with the electromagnetic field. The coupling between the acoustic and electromagnetic field in a porous media can be expressed by

$$J = \sigma E + L(-\nabla p + \omega^2 \rho_f u) \qquad (A.5)$$

$$-i\omega w = LE + (-\nabla p + \omega^2 \rho_f u)\kappa/\eta, \qquad (A.6)$$

where, J is the total electric current density, E is the electric field strength, u is the solid frame displacement, w is the fluid filtration displacement and p is the pore fluid pressure. L is the coupling coefficient, ρ_f and η are the density and the viscosity of the pore fluid, κ and σ are the dynamic permeability and conductivity of the porous medium respectively, ω is the angular frequency. The detailed expressions of L, κ are given by Pride (1994). In our numerical simulation, the L value is calculated by using a porous formation with the medium parameters listed in the table A.1.

	Porosity (%)	Ks (GPa)	Solid density (kg/m^3)	Solid Vp (m/s)	Solid Vs (m/s)	Permeability (darcy)
Formation	20	35	2600	2000	1200	1
Pore fluid density = 1000 (kg/m^3)			Pore fluid viscosity =0.001 Pa .S			
Pore fluid permittivity = 80 ε_0 (vacuum permittivity)			Formation permittivity = 4 ε_0 (vacuum permittivity)			

Table A.1 Medium properties used in the calculation of the coupling coefficient L

Under the assumption that the influence of the converted electric field on the propagation of the elastic waves can be ignored (Hu et al., 2000; Hu and Liu, 2002; Chi et al., 2005), we can further reduce the equation $(A.6)$ to

$$-i\omega w = (-\nabla p + \omega^2 \rho_f u)\kappa/\eta \qquad (A.7)$$

We can express the electric field as the gradient of the electric potential

$$E = -\nabla \phi. \qquad (A.8)$$

Taking the divergence of equation $(A.5)$ and using equation $(A.8)$ with the generalized

Ampere's law, we can have

$$J = \sigma E + L(-\nabla^2 p + \omega^2 \rho_f \nabla \cdot u) \qquad (A.9)$$

Since $\nabla \cdot u = \nabla^2 \varphi$, where φ is the displacement potential of the gradient field, equation $(A.9)$ can be written as

$$\nabla^2 \phi = (L/\sigma)(-\nabla^2 p + \omega^2 \rho_f \nabla^2 \varphi). \qquad (A.10)$$

To solve the equation $(A.10)$ in the wavenumber domain, we get

$$\phi = A \cdot K_n(kr) + (L/\sigma)(-p + \omega^2 \rho_f \varphi) \qquad (A.11)$$

where k is the axial wavenumber, $Kn(kr)$ is the modified Bessel function of nth order and A is the unknown coefficient for the electric field to be decided by the electric boundary conditions.

When the formation is homogenous and elastic, we can deduce the relationship between the coupled acoustic field potential and the electric field potential by deleting the pore pressure term in equation $(A.11)$ and get

$$\phi = A \cdot K_n(kr) + (L/\sigma)\omega^2 \rho_f \varphi. \qquad (A.12)$$

In the LWD geometry, using the expression of the displacement potentials in the elastic formation which is the $4th$ layer as indicated in the appendix A can be expressed as:

$$\begin{aligned} \phi_4 &= B_4 K_n(kp_4 r) \\ \chi_4 &= D_4 K_n(ks_4 r) \\ \Gamma_4 &= F_4 K_n(ks_4 r) \end{aligned} \qquad (A.13)$$

and the displacement potential ϕ_4 is the φ in equation $(A.10)$, $(A.11)$ and $(A.12)$.

In terms of potentials, the radial displacement component u_r in the elastic formation can be expressed as:

$$u_r = \frac{\partial \phi_4}{\partial r} + \frac{1}{r}\frac{\partial \chi_4}{\partial \theta} + \frac{\partial^2 \Gamma_4}{\partial r \partial z}. \qquad (A.14)$$

Combing the $(A.13)$ and $(A.14)$, we can get

$$u_r = B_4 K_n^{/}(kp_4 r) + \frac{n}{r} D_4 K_n(ks_4 r) + iks_4 F_4 K_n^{/}(ks_4 r). \qquad (A.15)$$

Substituting $(A.13)$ into $(A.12)$ and $(A.14)$ into $(A.9)$, using the relationship in $(A.8)$, we

can get the expression for the potential ϕ_{wall}, radial strength $E_{r\,wall}$ and the streaming current density J_{wall} of electric field along the elastic borehole wall

$$\begin{aligned}
\phi_{wall} &= AK_n(kr) + (L/\sigma)\omega^2\rho_f B_4 K_n(kp_4 r) \\
E_{rwall} &= \frac{-\partial\phi_{wall}}{\partial r} = -AK_n^{/}(kr) - (L/\sigma)\omega^2\rho_f B_4 K_n^{/}(kp_4 r) \\
J_{wall} &= -\sigma AK_n^{/}(kr) + L\omega^2\rho_f\left[\frac{n}{r}D_4 K_n(ks_4 r) + iks_4 F_4 K_n^{/}(ks_4 r)\right]
\end{aligned} \quad . \qquad (A.16)$$

Under the quasi-static assumption, the electric field in the borehole satisfies the Laplace's equation (Hu and Liu, 2002), the solution for the potential ϕ_{flul}, radial strength $E_{r\,flu}$ and the streaming current density J_{flu} is

$$\begin{aligned}
\phi_{flu} &= BI_n(kr) + CK_n(kr) \\
E_{rflu} &= \frac{-\partial\phi_{flu}}{\partial r} = -BI_n^{/}(kr) - CK_n^{/}(kr) \\
J_{flu} &= -\sigma\frac{\partial\phi_{flu}}{\partial r} = -\sigma\left[BI_n^{/}(kr) + CK_n^{/}(kr)\right]
\end{aligned} \qquad (A.17)$$

where B and C are the coefficients to be decided by the electric boundary conditions as well.

A.3 Electric boundary conditions in the LWD seismoelectric conversion

To solve the three coefficients A, B and C in the above expressions for the converted electric fields along the borehole wall (equation $(A.16)$) and in the borehole fluid (equation $(A.17)$), we apply the following three boundary conditions. On the borehole wall where $r = r_3$, we have

$$\begin{aligned}
\phi_{wall} &= \phi_{flu} \\
J_{wall} &= J_{flu}
\end{aligned} \quad . \qquad (A.18)$$

At the tool surface where $r = r_2$, we use the condition that the radial current density or the radial electric field strength (since they only differ in the multiplication of a conductivity) is equal to zero

$$E_{flu}(r_2) = 0\,. \qquad (A.19)$$

Substituting equation $(A.16)$ and $(A.17)$ into the three boundary conditions, we could

rewrite the boundary conditions in the matrix formation as following

$$\begin{bmatrix} \frac{-I_n'(kr_2)}{K_n'(kr_2)}K_n(kr)+I_n(kr) & -K_n(kr) \\ \frac{-I_n'(kr_2)}{K_n'(kr_2)}K_n'(kr)+I_n'(kr) & -K_n'(kr) \end{bmatrix} \begin{bmatrix} B \\ A \end{bmatrix} = \begin{bmatrix} (L/\sigma)\omega^2\rho_f B_4 K_n(kp_4 r) \\ -(L/\sigma)\omega^2\rho_f \left[\frac{n}{r} D_4 K_n(ks_4 r) + iks_4 F_4 K_n'(ks_4 r) \right] \end{bmatrix}$$

. $(A.20)$

From equation $(A.20)$, we could get A and B after we solve the acoustic coefficients B_4, D_4 and F_4 by applying the LWD acoustic mechanical boundary conditions. Electric coefficient C can be calculated by substituting B into equation $(A.19)$. Once A, B and C are all determined, the electric field both along the borehole wall and within the borehole fluid can be determined.

A.4 The synthetic waveforms of the LWD acoustic and seismoelectric signal

The formation properties are the same as the lab formation. The four layer model we use to simulate the LWD process is listed in the Table A.2. A scaling factor of 17 is used to scale the lab tool to the real LWD tool. The source wavelet in the experiment is a square wave with a center frequency of 100 kHz. Scaling the 100kHz center frequency to the modeling, we use a Ricker wavelet with the center frequency of 6kHz as a source. The formulae in both acoustic and electric calculations are expressed in the wavenumber domain, thus we use the discrete wavenumber method (Bouchon and Schimitt, 1989; Bouchon, 2003) to do the modeling.

Figure A.1 and Figure A.2 show the calculated monopole and dipole waveforms using the fast formation parameters of our lab experiment. Solid curves are the acoustic signals and the dotted curves are the electric signals. (A-A) is the radiating electromagnetic wave in both figures. The figures are scaled back to the lab borehole tool scale with the first trace located at $z = 0.098$ m and the spacing is 0.012 m as shown in Figure 2.

In figure A.1, (B-B) is the formation compressional wave, (C-C) is the monopole tool wave and (D-D) represents the formation shear wave, (E-E) is the Stoneley wave. We use the same semblance method to analyze the wave modes in the acoustic and electric waveforms as we did for the experiment data. The time domain semblances for the monopole acoustic and electric waveforms are shown in Figure A.3 and Figure A.4 respectively. The absence of the monopole tool mode which is indicated by the first big block in Figure A.3 can be observed very clearly in the semblance of the electric signal (Figure A.6).

The same phenomena can be observed for the dipole case. In Figure A.2, (B-B), (C-C), (D-D) are the 2nd order dipole formation flexural wave, dipole tool wave and 1st order dipole formation flexural wave, respectively. The absence of the dipole tool mode, which is indicated by the second big block in Figure A.5, can be observed very clearly in the

semblance of the electric signal (Figure A.6).

	P-velocity	S-velocity	Density	Outer radius
Inner fluid	$1500\,m/s$	-------	$1000\,kg/m^3$	0.024m
Tool (Composite)	$4185\,m/s$	$2100\,m/s$	$7700\,kg/m^3$	0.085m
Outer fluid	$1500\,m/s$	-------	$1000\,kg/m^3$	0.11m
Fast Formation	$4660\,m/s$	$2640\,m/s$	$2100\,kg/m^3$	∞

Table A.2 LWD lab borehole model used in acoustic and seismoelectric modeling

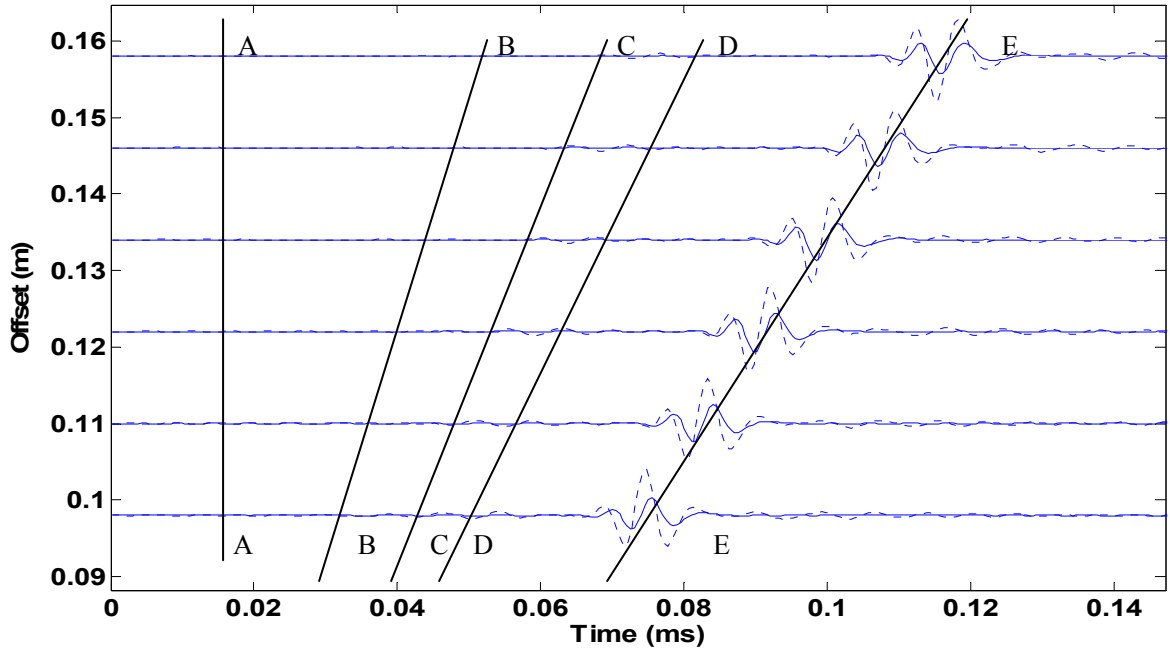

Figure A.1 The monopole waveforms of the normalized acoustic pressure (solid curves) and the normalized electric field strength (dotted curves) for laboratory fast formation (A, B, C, D, E indicate the different arrivals described in the text).

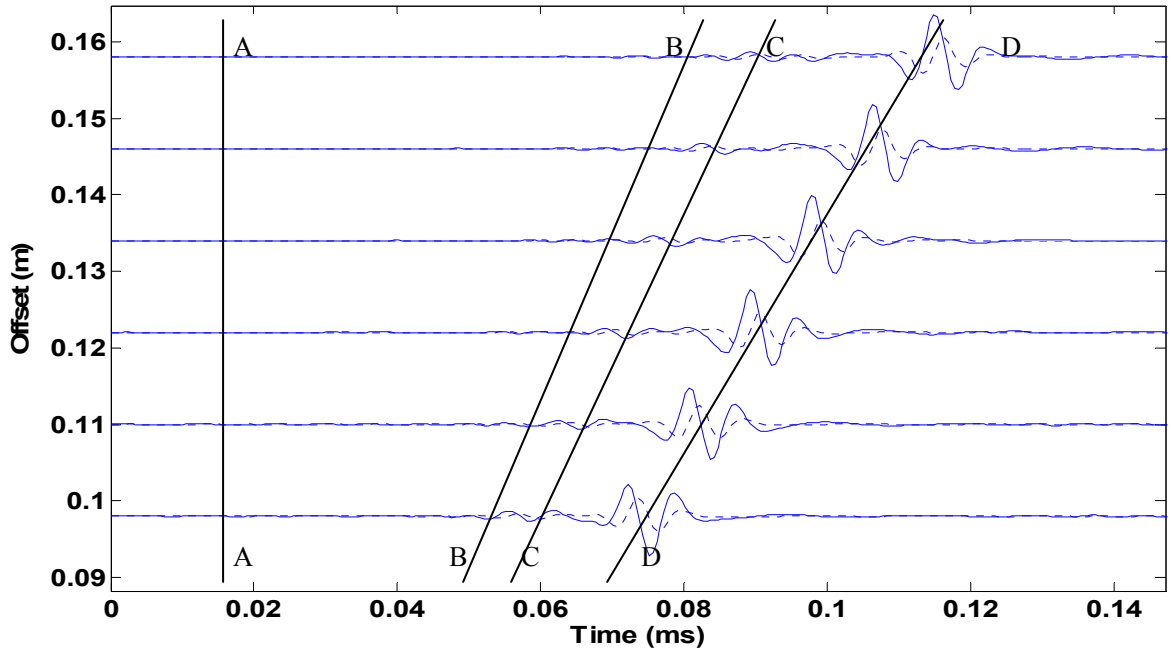

Figure A.2 The dipole waveforms of the normalized acoustic pressure (solid curves) and the normalized electric field strength (dotted curves) for laboratory fast formation (A, B, C, D indicate the different arrivals described in the text).

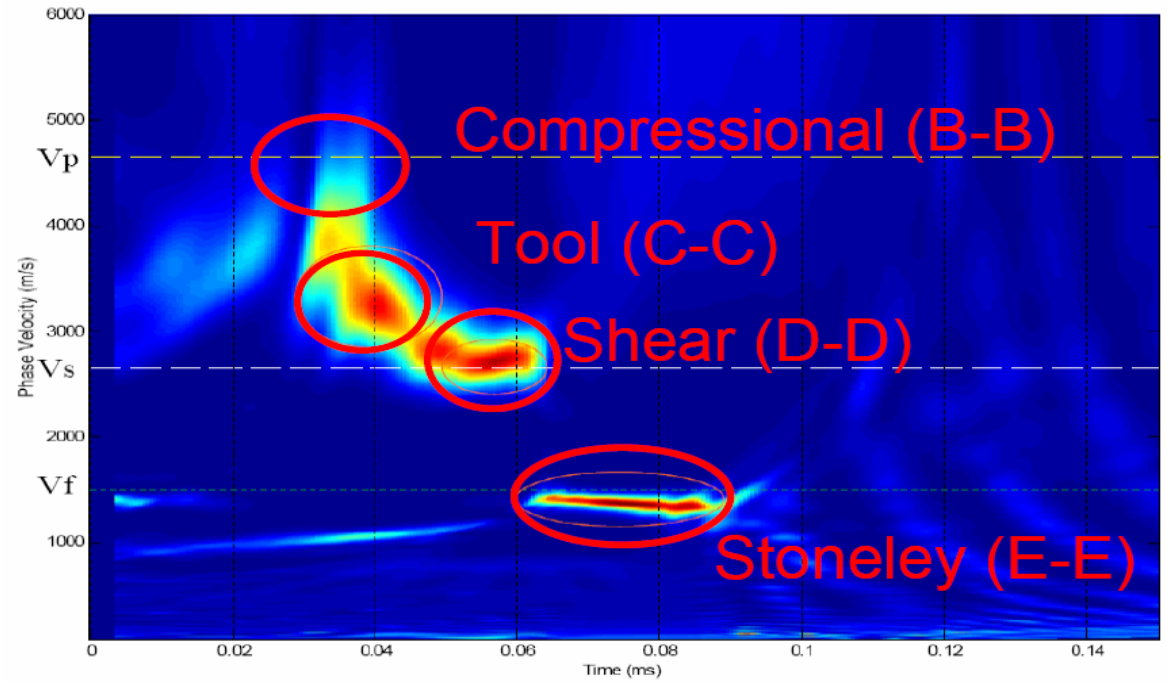

Figure A.3 The time domain semblance of the monopole acoustic waveforms in figure 4.6. (The three circles indicates the monopole tool wave, shear wave and stonely wave respectively from top to bottom.Compressional wave is not very clear in this figure. Vp stands for the formation P wave velocity, Vs for S wave velocity, Vf for fluid wave velocity.)

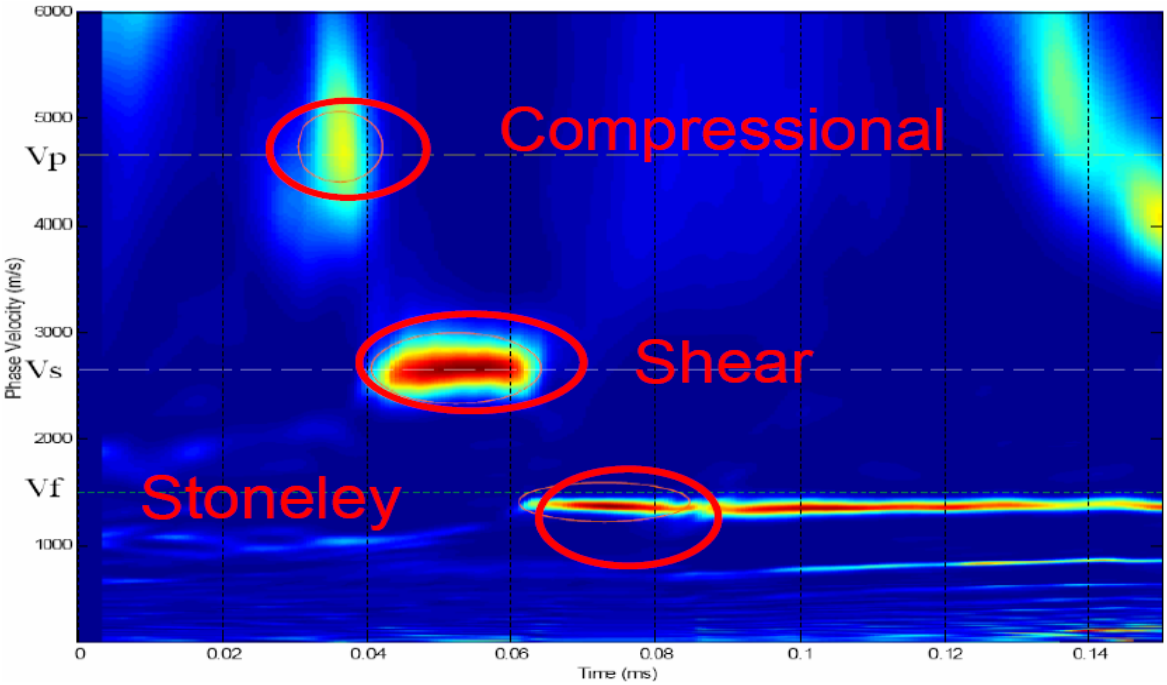

Figure A.4 The time domain semblance of the monopole electric waveforms in figure 4.6. (The three circles indicates the monopole compressional wave, shear wave and stonely wave respectively from the top to bottom. Vp stands for the formation P wave velocity, Vs for S wave velocity, Vf for fluid wave velocity.)

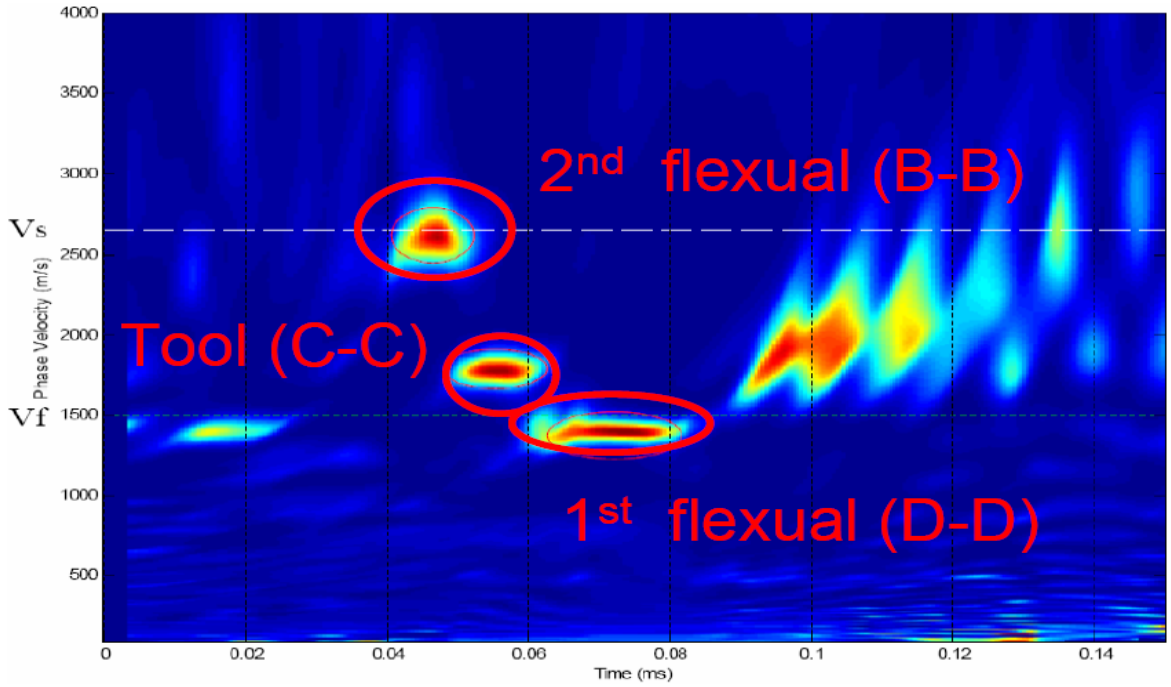

Figure A.5 The time domain semblance of the dipole acoustic waveforms in figure 4.7. (The three circles indicates the 1st order dipole formation flexural wave, tool wave and 2nd order formation flexuraly wave respectively from the above to the bottom. Vs stands for formation S wave velocity. Vf for fluid wave velocity.)

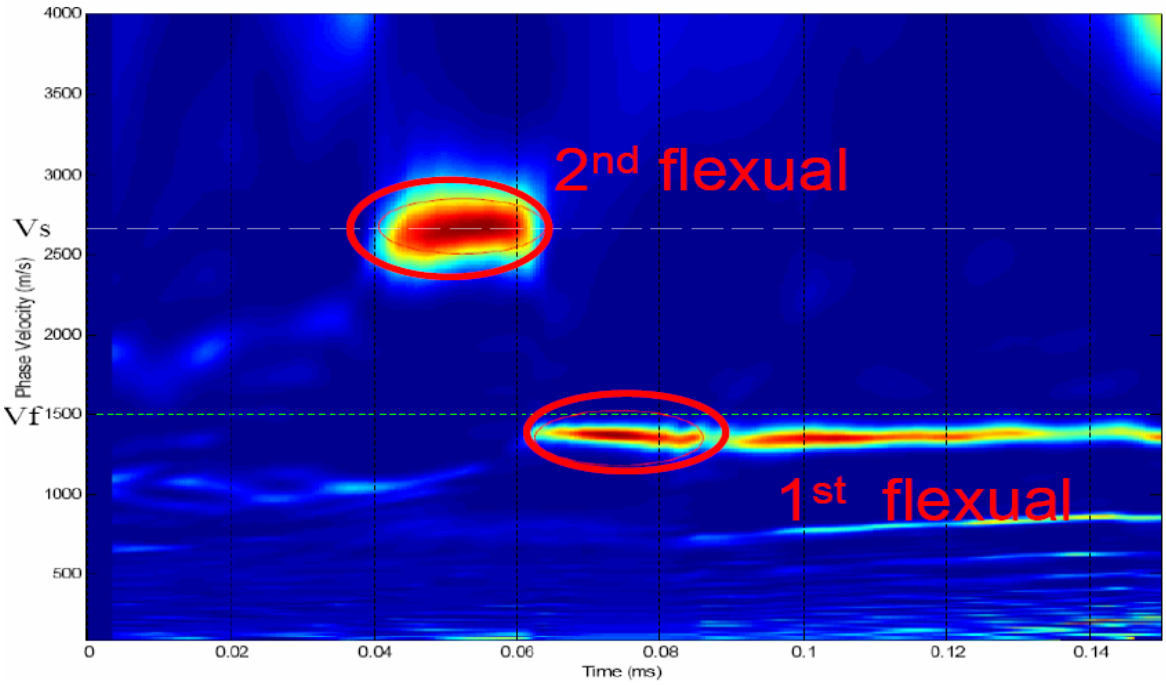

Figure A.6 The time domain semblance of the dipole electric waveforms in figure 4.7. (The two circles indicates the 1st order dipole formation flexural wave and 2nd order formation flexuraly wave respectively from the above to the bottom. Vs stands for formation S wave velocity, Vf for fluid wave velocity.)

5. Reference

Aki, K. and Richards, P. G. (1980). *Quantitative Seismology, Theory and Methods.* W. H. Freeman and Co., San Francisco.

Aron, J., Chang, S., Dworak, R., Hsu, K., Lau, T., Masson, J., Mayes, J., McDaniel, G., Randall, C., Kostek, S., and Plona, T. (1994). Sonic compressional measurements while drilling. *SPWLA 35th Annual Logging Symposium.*

Biot, M. A. (1941). General theory of three-dimensional consolidation. *J. Applied Phys.,* 12, 155-164.

Biot, M. A. (1956a). Theory of propagation of elastic waves in a fluid-saturated porous solid. I. Low-frequency range. *J. Acoust. Soc. Am.,* 28, 168-178.

Biot, M. A. (1956b). Theory of propagation of elastic waves in a fluid-saturated porous solid. II. High-frequency range. *J. Acoust. Soc. Am.,* 28, 179-191.

Biot, M. A. (1962). Mechanics of deformation and acoustic propagation in porous media. *J. Applied Phys.,* 33, 1482-1489.

Biot, M. A. (1952). Propagation of elastic waves in a cylindrical bore containing a fluid. *J. Appl. Phys.,* 23, 997-1005.

Bockris, J. and Reddy, A. K. N. (2000). *Modern electrochemistry*. Plenum Press, New York.

Bouchon, M. and Schimitt, D. (1989). Full-wave acoustic logging in an irregular borehole. *Geophysics*, 54, 758-765.

Bouchon, M. (2003). A review of the discrete wavenumber method. *Pure and Applied Geophysics.* 160, 445-465.

Butler, K. E. and Russell, R. D. (1993). Subtraction of powerline harmonics from geophysical records. *Geophysics*, 58, 889-903.

Butler, K. E. and Russell, R. D. (2003). Cancellation of multiple harmonic noise series in geophysical records. *Geophysics*, 68, 1083-1090.

Chen, S. T. and Eriksen, E. A. (1991). Compressional and shear-wave logging in open and cased holes using a multipole tool. *Geophysics,* 61, 437-443.

Cheng, C. H. and Toksöz, M. N. (1981). Elastic wave propagation in a fluid-filled borehole and synthetic acoustic logs. *Geophysics,* 46, 1042-1053.

Cheng, N. Y. and Cheng, C. H. (1996). Estimation of formation velocity, permeability, and shear-wave

anisotropy using acoustic logs. *Geophysics,* 56, 550-557.

Chi, S. H, Toksöz, M. N., and Xin, Z. (2005). Theoretical and numerical studies of seismoelectric conversions in boreholes. *Submitted to Proceeding of the 17th International Symposium of Nonlinear Acoustics, Pennsylvania State University. Published by American Institute of Physics.*

Chi, S. H., Zhu, Z., Rao, V. N. R., and Toksöz, M. N. (2005). Higher order modes in acoustic logging while drilling. *Borehole Acoustic and Logging / Reservoir Delineation Consortia Annual Report, MIT.*

Cittá, F., Russell, C., Deady, R., and Hinz D. (2004). Deepwater hazard avoidance in a large top-hole section using LWD acoustic data. *The Leading Edge*, 23, 566-573.

Desbrandes, R. (1985). *Encyclopedia of well logging.* Gulf Publishing Company.

Dukhin, S. S. and Derjaguin, B. V. (1974). Electrokinetic phenomena. John Wiley and Sons, Inc.

Esmersoy, C., Hawthorn A., Durrand, C., and Armstrong P. (2005). Seismic MWD: Drilling in time, on time, it's about time. *The Leading Edge*, 24, 56-62.

Fitterman, D. V. (1979). Relationship of the self-potential Green's function to solutions of controlled source direct-current potential problems. *Geophysics,* 44, 1879-1881.

Haartsen, M. W. (1995). *Coupled electromagnetic and acoustic wavefield modeling in poro-elastic media and its applications in geophysical exploration.* Ph.D. thesis, Massachusetts Institute of Technology, Department of Earth, Atmospheric and Planetary Sciences.

Haartsen, M. W., Zhu, Z., and Toksöz, M. N. (1995). Seismoelectric experimental data and modeling in porous layer models at ultrasonic frequencies. In *Expanded Abstract, 65th Ann. Internat. Mtg*., pages 26-29. Soc. Expl. Geophys.

Haartsen, M. W. and Pride, S. R. (1997). Electroseismic waves from point source in layered media. *J. Geophys Res.,* 102, 24745-24769.

Hsu, C. J., Kostek, S., and Johnson, D. L. (1997). Tube waves and mandrel modes: experiment and theory. *J. Acoust. Soc. Am.,* 102, 3277-3289.

Hu, H. S., Wang, K. X., and Wang, J. N. (2000). Simulation of an acoustically induced electromagnetic field in a borehole embedded in a porous formation. *Borehole Acoustic and Logging / Reservoir Delineation Consortia Annual Report, MIT.*

Hu, H. S. and Liu, J. Q. (2002). Simulation of the converted electric field during acoustoelectric logging. *SEG Int'l Exposition and 72nd Annual Meeting, Salt Lake City, Utah, 2002, October 6-11.*

Huang, X. (2003). *Effects of tool positions on borehole acoustic measurement: a stretched grid finite difference approach.* Ph.D. thesis, Massachusetts Institute of Technology, Department of Earth, Atmospheric and Planetary Sciences.

Hunter, Robert J. (2001). *Foundations of colloid science*. Oxford University Press, New York

Ishido, T. and Mizutani, H. (1981). Experimental and theoretical basis of electrokinetic phenomena in rock-water systems and its applications to geophysics. *J. Geophys Res.,* 86, 1763-1775.

Ivanov, A. G. (1940). The electroseismic effect of the second kind. *Izvestiya Akademii Nauk SSSR, Ser. Geogr. Geofiz*., 5, 699-727.

Joyce, B., Patterson, D., Leggett, J. V., and Dubinsky, V. (2001). Introduction of a new omni-directional acoustic system for improved real-time LWD sonic logging-tool design and field test results. *SPWLA 42nd Annual Logging Symposium.*

Kimball, C. V., and Marzetta, T. L. (1984). Semblence processing of borehole acoustic array data. *Geophysics*, 49, 274-281.

Kurkjian, A. L. and Chang, S. K. (1986). Acoustic multipole sources in fluid-filled boreholes. *Geophysics*, 51, 148-163.

Li, S. X., Pengra, D. B., and Wang, P. Z. (1995). Onsagers reciprocal relation and the hydraulic permeability of porous media. *Phys. Rev. E,* 51, 5748-5751.

Loren, B., Perrier, F., and Avouac, J. P. (1999). Streaming potential measurements 1. Properties of the electrical double layer from crusted rock samples. *J. Geophys Res.,* 104, 17857-17877.

Market, J., Althoff, G., Barnett, C., and Deady, R. (2002). Processing and quality control of lwd dipole sonic measurements. *SPWLA 43rd Annual Logging Symposium, Osio, Japan.*

Markov, M. G. and Verzhbitskiy, V. V. (2004). Simulation of the electroseismic effect produced by an acoustic multipole source in a fluid-filled borehole. *SPWLA 43rd Annual Logging Symposium, 2004, June 6-9,* paper VV.

Minear, J., Birchak, R., Robbins, C., Linyaev, E., and Mackie, B. (1995). Compressional wave slowness measurement while drilling. *SPWLA 36th Annual Logging Symposium.*

Mikhailov, O. V. (1998). *Borehole electroseismic phenomena.* Ph.D. thesis, Massachusetts Institute of Technology, Department of Earth, Atmospheric and Planetary Sciences.

Mikhailov, O. V., Queen, J., and Toksöz, M. N. (2000). Using borehole electroseismic measurements to detect and characterize fractured (permeable) zones. *Geophysics*, 65, 1098-1112.

Nolte B., Rao, V. N. R., and Huang, X. (1997). Dispersion analysis of split flexural waves. *Borehole Acoustic and Logging / Reservoir Delineation Consortia Annual Report, MIT.*

Peterson, E. W. (1974). Acoustic wave propagation along a fluid-filled cylinder. *J. Appl. Phys.,* 45, 3340-3350.

Pride, S. R. and Morgan, R. D. (1991). Electrokinetic dissipation induced by seismic waves. *Geophysics*, 56, 914-925.

Pride, S. R. (1994). Governing equations for the coupled electromagnetics and acoustics of porous media. *Phys. Rev. B*, 50, 15678-15696.

Pride, S. R. and Haartsen, M. W. (1996). Electroseismic wave properties. *J. Acoust. Soc. Am.,* 100, 1301-1315.

Rao, V. N. R., Burns, D. R., and Toksöz, M. N. (1999). Models in LWD applications. *Borehole Acoustic and Logging / Reservoir Delineation Consortia Annual Report, MIT.*

Rao, V. N. R. and Toksöz, M. N. (2005). Dispersive wave analysis – method and applicatoins. *Borehole Acoustic and Logging / Reservoir Delineation Consortia Annual Report, MIT.*

Reppert, P. M., Morgan, F. D., Lesmes, D. P., and Jouniaux, L. (2001). Frequency-dependent streaming potentials. *Journal of Colloid and Interface Science,* 234, 194-203.

Rover, W., Rosenbaum, J., and Ving, T. (1974). Acoustic waves from an impulsive source in a fluide-filled borehole. *J. Acoust. Soc. Am.,* 55, 1144-1157.

Russell, R. D., Butler, K. E., Kepic, A. W., and Maxwell, M. (1997). Seismoelectric exploration. *The Leading Edge*, 16, 1611-1615.

Schimitt, D. P. (1986). Full wave synthetic acoustic logs in saturated porous media. Part I. A review of Biot's theory . *ERL Full Waveform Acoustic Logging Consortium Annual Report,* 1986, 105-153.

Schimitt, D. P. (1986). Full wave synthetic acoustic logs in saturated porous media. Part II. Simple configuration . *ERL Full Waveform Acoustic Logging Consortium Annual Report,* 1986, 175-208..

Schimitt, D. P. and Cheng, C. H. (1987). Shear wave logging in (multilayered) elastic formations: an overview. *ERL Full Waveform Acoustic Logging Consortium Annual Report,* 1987, 213-237.

Schimitt, D. P. (1988). Transversely isotropic saturated porous formations: I. Theoretical developments and (quasi) body wave properties. *ERL Full Waveform Acoustic Logging Consortium Annual Report,* 1988, 247-290.

Schimitt, D. P. (1989). Acoustic multipole logging in transversely isotropic poroelastic formations. *J. Acoust. Soc. Am.,* 86, 2397-2421.

Segesman, F. (1962). New SP correction charts. *Geophysics,* 27, 815-828.

Segesman, F. F. (1980). Well-logging method. *Geophysics,* 45, 1667-1684.

Sill, W. R. (1983). Self-potential modeling from primary flows. *Geophysics,* 48, 76-86.

Sprunt, E. S., Mercer, T. B., and Djabbarah, N. F. (1994). *Geophysics,* 59, 707-711.

Tang, X. M. and Cheng, C. H. (1993). Effects of a logging tool on the Stoneley waves in elastic and porous boreholes. *Log Analyst*, 34, 46-56.

Tang, X. M., Wang, T., and Patterson, D. (2002). Multipole acoustic logging-while-drilling. *SEG Technical Program and Expanded Abstract,* 2002, 364-367

Tang, X. M., Dubinsky, V., Wang, T., Bolshakov, A., and Patterson, D. (2002). Shear-velocity measurement in the logging-while-drilling environment: modeling and field evaluations. *SPWLA 43rd Annual Logging Symposium, 2002, June 2-5,* paper RR..

Tang, X. M. and Cheng, C. H. (2004). *Quantitative borehole acoustic methods*. Elsevier, Science Publishing Co., Oxford.

Thompson, A. and Gist, G. (1993). Geophysical applications of electrokinetic conversion. *The Leading Edge*, 12, 1169-1173.

Tsang, L. and Rader, D. (1979). Numerical evaluation of transient acoustic waveforms due to a point source in a fluid-filled borehole. *Geophysics*, 44, 1706-1720.

White, J. E. and Zechman, R. E. (1968). Computed response of an acoustic logging tool. *Geophysics,* 33, 302-310.

White, J. E. (1983). *Underground sound*. Elsevier, Science Publishing Co., Amsterdam.

Zhu, Z. and Toksöz, M. N. (1996). Experimental studies of electrokinetic conversion in fluid-saturated porous medium. In *Expanded Abstracts, 66th Ann. Internat. Mtg*., pages 1699-1702. Soc. Expl. Geophys.

Zhu, Z. and Toksöz, M. N. (1997). Experimental studies of electrokinetic conversion in fluid-saturated borehole models. In *Expanded Abstracst, 67th Ann. Internat. Mtg*., pages 334-337. Soc. Expl. Geophys.

Zhu, Z. and Toksöz, M. N. (1998). Seismoelectric and seismomagnetic measurements in fractured borehole models. In *Expanded Abstract, 69th Ann. Internat. Mtg*., pages 144-147. Soc. Expl. Geophys.

Zhu, Z., Haartsen, M. W., and Toksöz, M. N. (1999). Experimental studies of electrokinetic conversions in fluid-saturated borehole models. *Geophysics*, 64, 1349-1356.

Zhu, Z., Haartsen, M. W., and Toksöz, M. N. (2000). Experimental studies of electrokinetic conversions in fluid-saturated porous media. *J. Geophys Res.,* 105, 28055-28064.

Zhu, Z. and Toksöz, M. N. (2003). Crosshole seismoelectric measurements in borehole models with fractures. *Geophysics*, 68, 1519-1524.

Zhu, Z., Rao, V. N. R., and Burns, D. R., and Toksöz, M. N. (2004). Experimental studies of multipole logging with scaled borehole models. *Borehole Acoustic and Logging / Reservoir Delineation Consortia Annual Report, MIT.*

Zhu, Z., Chi, S. H., and Toksöz, M. N. (2005). Experimental and theoretical studies of seismoelectric effects in boreholes. *Borehole Acoustic and Logging / Reservoir Delineation Consortia Annual Report, MIT.*

Xin Z., Zhu, Z., Chi, S. H., Rao, V. N. R., and Toksöz, M. N. 2005.An experimental study of seismoelectric signals in logging while drilling. *Borehole Acoustic and Logging / Reservoir Delineation Consortia Annual Report, MIT.*

Xin Z. 2005. A study of seismoelectric signals in measurement while drilling. M.S. thesis, Massachusetts Institute of Technology, Department of Earth, Atmospheric and Planetary Sciences.